Soft Matter

PAPER

View Article Online
View Journal | View Issue

Cite this: *Soft Matter*, 2018, **14**, 2254

Structural evolution and stability of non-crosslinked fiber networks with inter-fiber adhesion

R. C. Picu * and A. Sengab

Received 28th December 2017,
Accepted 1st March 2018

DOI: 10.1039/c7sm02555f

rsc.li/soft-matter-journal

Adhesion plays an important role in the mechanics of nanoscale fibers such as various biological filaments, carbon nanotubes and artificial polymeric nanofibers. In this work we study assemblies of non-crosslinked filaments and characterize their adhesion-driven structural evolution and their final stable structure. The key parameters of the problem are the network density, the fiber length, the bending stiffness of fibers and the strength of adhesion. The system of fibers self-organizes in one of three types of structures: locked networks, in which fibers remain in the as-deposited state, cellular networks, in which fibers form bundles and these organize into a larger scale network, and disintegrated networks, in which the network of bundles becomes disconnected. We determine the parametric space corresponding to each of these structures. Further, we identify a triangular structure of bundles, similar to the Plateau triangle occurring in foams, which stabilizes the network of bundles and study in detail the stabilization mechanism. The analysis provides design guidelines and a physical picture of the stability and structure of random fiber networks with adhesion.

1. Introduction

Many artificial and biological soft materials are fibrilar, either being made from a dense packing of filaments or having a fiber network as their main structural component. Examples include various types of non-wovens, fiber-based insulation and filtration materials, and a variety of hygiene products. Collagen is one of the main structural materials in the human and animal bodies and is present in the form of bundles of filaments of a range of diameters.[1,2]

Fiber bundling in random fibrous materials is broadly observed. Elastocapillarity represents the interaction of liquid–air or liquid–liquid interfaces with elastic structures.[3] Capillarity organizes fibrils into structures[4] and may be used to produce a variety of effects in soft matter, as reviewed in ref. 5. If the structure remains wet, capillary forces are sufficient to hold the fiber bundles together. If it is dried, adhesion stabilizes the bundled structure;[6] an analysis of this process is presented by Cranford *et al.*[7] While the longer ranged capillary forces are more efficient in organizing fibrous structures into fiber bundles, adhesion-driven bundling also takes place in the dry state.[8]

Aggregation in colloidal particle suspensions is produced by inter-particle interactions and hydrodynamic forces.[9] Suspensions of rigid and flexible fibers undergo flocculation as the concentration increases. The formation of filament bundles was observed in dense suspensions of actin[10] and collagen[11] and the process was discussed theoretically by Zilman and Safran[12] using a mean field model. This theoretical work outlines a sol–gel transition followed by another transition to a bundled state as the fiber concentration increases or/and temperature decreases. Inter-particle interactions lead to the modification of the rheological response in concentrated suspensions of filaments, including the occurrence of a pseudo-yield stress[13] and shear thinning.[14]

Adhesion is particularly strong between carbon nanotubes (CNT). Buckypaper is a quasi-two-dimensional material similar to regular paper, made from CNTs deposited on a substrate. The CNTs self-organize under the action of adhesive forces leading to the formation of CNT bundles[15–18] whose size and structure depends on the bending stiffness (*i.e.* whether the buckypaper contains single wall or multiwall CNTs) and the length of the filaments.

While substantial work was dedicated to the mechanics of cross-linked networks of fibers both in the mechanics of materials and physics literature (see reviews[19,20]), the mechanical behavior of non-cross-linked filament packings was studied to a smaller extent.[21–25] Non-cross-linked filamentary structure mechanics is controlled by the deformation of fibers and their topological (excluded volume) interactions. The mechanical behavior of non-bonded assemblies of filaments in presence

Department of Mechanical, Aerospace and Nuclear Engineering, Rensselaer Polytechnic Institute, Troy, NY 12180, USA. E-mail: picuc@rpi.edu; Tel: +1 518 276 2195

of adhesive interactions is even less studied. Li and Kroger[26,27] studied numerically the structure and mechanical behavior of buckypaper. They observe intense bundling and conclude that for CNTs with weaker adhesion the structure is controlled by entanglements, while CNTs with stronger adhesion form bundles. The pore size of the respective structures could be controlled from 7 nm to 50 nm by increasing the bending stiffness of filaments. Volkov and Zhigilei[28] also simulated assemblies of CNTs and concluded that the resulting structures can be stabilized provided the CNT length is larger than a threshold value and, for systems of single wall CNTs, bending-buckling is considered in the model. A demonstration of the effect of adhesion between filaments on the overall mechanical behavior of the network was provided by Xu *et al.*[29] using random networks of long un-cross-linked CNTs. They observe strong energy dissipation under cyclic loading due to the bundling/unbundling of filaments. Since the system is athermal (mechanical behavior is not affected by thermal fluctuations), the measured system-scale storage and loss moduli are temperature independent in a broad range of temperatures. Simulations reproducing this result were presented by Li and Kroger.[30]

The present study is motivated by the limited understanding of the stability and mechanics of fiber networks of non-cross-linked filaments interacting adhesively. We focus on identifying the types of stable structures into which a quasi-two-dimensional fibrous network evolves under the action of adhesive forces. To this end, we first identify the system parameters of importance in this problem, and perform a parametric study to determine the stable network structures of interest. A numerical model is used for this purpose. We observe that fibers either remain locked in the as-deposited state, or evolve by bundling. The evolution can lead to either the full disintegration of the network into a set of large, isolated bundles, or to a network of fiber bundles. We find the range of parameters in which such networks of bundles exist. The essential contribution of this work is the identification of the structural element that stabilizes networks of bundles. This is a triangular feature that forms at the nodes of the network, resembling the Plateau triangles in foams. Given the importance of these constructs, we provide a comprehensive description of the mechanisms by which such triangles form and stabilize the network.

2. Problem definition

We consider ensembles of filaments of identical diameter, d_0, and length, L_0, made from the same linear elastic material of Young's modulus, E_0. The fibers are sufficiently large to be considered athermal and hence behave mechanically as beams of axial and bending rigidities E_0A_0 and E_0I_0, where A_0 and I_0 are the area and moment of inertia of the fiber cross-section. The torsional rigidity of fibers is less important in this problem in absence of chirality, since random networks do not store much strain energy in the torsional mode of the fibers.[20,31]

Inter-fiber adhesion is defined by the energy gain per unit area of contact when two surfaces are brought together, γ_0. In the case of cylindrical filaments, the contact is established over an area of width c_0. In absence of chirality or residual stress in fibers, the two cylinders in contact remain parallel. The Johnson–Kendall–Roberts (JKR) and the Derjaguin–Muller–Toporov (DMT) theories predict that $c_0 \sim (\gamma_0 d_0^2/E_0)^{1/3}$.[32–34] The adhesion energy per unit length of filament is $\gamma = \gamma_0 c_0$.[35]

Fibers are randomly deposited into a quasi-two-dimensional mat without fiber–fiber interpenetration. The structure is three-dimensional and the mat has finite thickness. We consider the limit of vanishing inter-fiber friction. It is convenient to describe the mat density, ρ, in projection on the mean plane of the mat as the total length of fiber per unit area of the projection. If the mat is thicker than 3–4 fiber diameters, a given fiber does not make contacts with all fibers it intersects in projection. This situation is qualitatively similar to that of thin mats and hence the concepts discussed here apply to both thin and thick initial structures.

The as-deposited mat is organized by the adhesive interactions between fibers. Bundles of closely packed parallel fibers form and organize further into a new network of bundles. The objective of this work is to define the structure and stabilization mechanism of networks of fiber bundles.

3. Computational model definition

The study of the evolution of a large number of fibers interacting adhesively requires a numerical approach. In this work we use a bead-spring model similar to that employed frequently in polymer physics to represent the coarse grained mechanics of polymeric molecules. Such model was used to represent CNT bundles.[4,27,30] Each filament is represented by a collection of spherical beads which interact along the filament through axial and angular potentials that mimic the axial and bending stiffness of the fiber. The stiffness of the harmonic axial potential is $k_a = E_0A_0/\sigma_a$, while the stiffness of the angular potential is $k_b = E_0I_0/\sigma_a$, where σ_a is the distance between consecutive bead centers along the filament.

Non-bonded interactions between beads not belonging to the same fiber are represented *via* Lennard-Jones (LJ) potentials of characteristic length σ and well depth, ε_0. These impose the excluded volume condition and represent the adhesive energy per unit length of contact between two straight and parallel fibers in equilibrium, γ.

The fiber parameters, γ, d_0 and E_0 are uniquely defined in this model by parameters σ, ε_0 and k_a (or k_b). d_0 is the equilibrium distance of a bead from the axis of an infinite straight fiber and, for the potentials used, is related to σ as $d_0 = 1.063\sigma$. Parameter γ is given by $\gamma = 7.11\varepsilon_0/\sigma$. The effective fiber modulus is defined by either k_a or k_b as $E_0 = 0.3k_a/\sigma$ or $E_0 = 4.8k_b/d_0^2\sigma$.

The discreteness of the filament representation renders the fiber surface rough, which may lead to undesirable interlocking and friction. In order to minimize this effect, the density of beads along the filament is increased to 4 beads per fiber segment of aspect ratio 1, $\sigma_a = d_0/4$. We evaluated the resulting

roughness by considering two relaxed parallel chains in adhesive contact which were displaced axially relative to each other. The fluctuations of adhesion energy during such sliding are within 0.01% of the mean.

The mat of fibers is created by depositing fibers on a plane with random orientations and random positions of their centers of mass in a square domain of size $L \times L$, with $L > 2L_0$ in all cases. Periodic boundary conditions are imposed in the plane of the mat and zero tractions are imposed in the direction perpendicular to the plane of the mat. Fibers do not interact adhesively or frictionally with the support plane, which is removed after the mat is constructed and relaxed.

In the production phase, the system evolves under the action of inter-fiber adhesion forces, subjected to periodic boundary conditions in the plane of the mat. This represents a system of infinite 2D extent and of constant average density. The system is evolved with molecular dynamics. Various temperatures up to 300 K are used in separate simulations in order to test the effect of this parameter on the resulting structure. No significant differences are observed for the set of energetic parameters used in these simulations; this is expected given the athermal nature of the system.[29,30] Simulating at higher temperatures is desirable in order to reduce the computational cost. Since at finite temperatures one cannot exclude aging effects, *i.e.* the very slow, thermally activated evolution of the system, we run long simulations with stopping criterion being the variation of the total energy of the system by less than 10^{-5}% per integration time step. However, the stability of the system is evaluated based on theoretical considerations presented in Section 5.

Simulations are performed using LAMMPS from Sandia National Labs.[36] We use the Nose–Hoover thermostat and the velocity Verlet integration algorithm. All simulations are performed on a massively parallel computer at the RPI Center for Computational Innovation.

4. Results and discussion

4.1 Network evolution modes

Simulations are used to evolve the system of fibers and various sets of the control parameters are used in separate simulations. Fig. 1 shows two examples of system evolution. Two values of the non-dimensional parameter ρL_0 are selected, $\rho L_0 = 24.8$ and $\rho L_0 = 99.25$, which correspond to systems of same density and different fiber length. In Fig. 1, the images on the first line show the two dimensional (projected) view of the as-deposited networks, while those on the second line show the corresponding final states. In the as-deposited state each line represents an individual filament, while a network of bundles forms at later stages. It is observed that the network of low ρL_0 disintegrates, *i.e.* fibers bundle until the resulting network of bundles loses connectivity. In this limit, the network decomposes in a set of individual bundles of length bounded below by L_0. The system of higher ρL_0 reaches a stable cellular structure whose total energy remains constant in time.

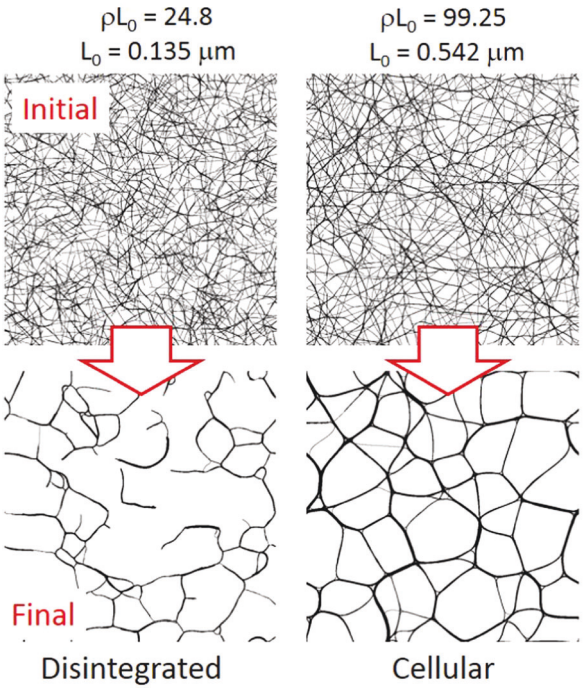

Fig. 1 Initial and final structures for two networks of same density but different fiber length, L_0. The initial network of short fibers disintegrates, while that of longer fibers forms a cellular structure.

We analyze the network evolution using two parameters: the average cell diameter, $\bar{d}$, and the average bundle size, $\bar{n}$. The cell diameter is computed as $d = \sqrt{A}$, where A is the projected area of a cell (inset to Fig. 2). This parameter is evaluated by processing images similar to that of the cellular structure in Fig. 1. The bundle size represents the number of fibers forming a bundle.

Fig. 2 shows the variation of the normalized inverse $\bar{d}$, $L_0/\bar{d}$, *versus* $\bar{n}$ for four representative systems. This figure shows the main features of structural evolution. In the initial state, $\bar{n} = 1$,

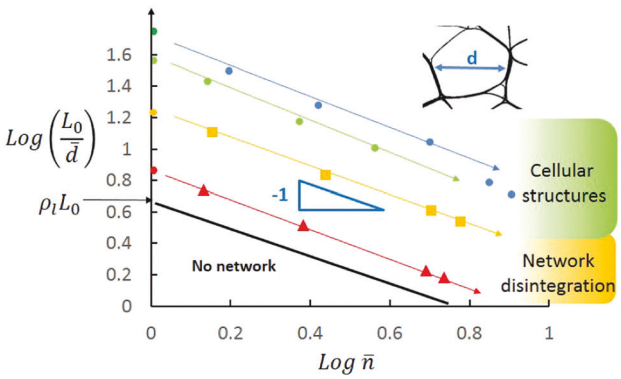

Fig. 2 The evolution of the structure of four initial networks of different ρ and L_0. The structure is described in terms of the mean cell size, $\bar{d}$, and the mean bundle size, $\bar{n}$. Systems in the as-deposited conditions are not bundled and correspond to points on the vertical axis ($\bar{n} = 1$). System evolution leads either to the full disintegration of the network or to a cellular structure. The inset defines the approximate cell diameter.

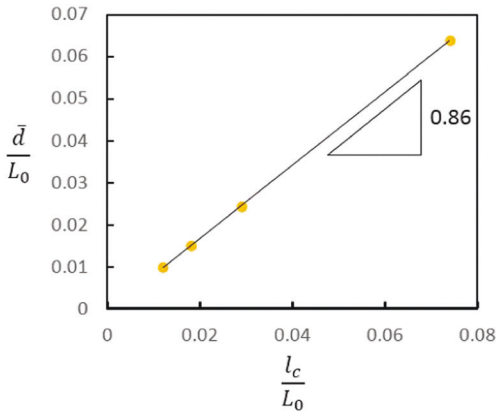

Fig. 3 Relation between the mean cell size, $\bar{d}$, and the mean segment length, l_c, for 2D Mikado networks in the as-deposited, un-bundled state.

the network is in the as-deposited state (initial states of Fig. 1) and can be described using concepts relevant for two-dimensional Mikado networks. In these networks, the mean segment length, l_c, is related to the density through the Kallmes–Corte relation, $l_c = \pi/2\rho$.[37] Furthermore, in the initial state, $\bar{d}$ varies linearly with l_c as:

$$\bar{d} = 0.86 l_c. \quad (1)$$

This relationship is supported by the data shown in Fig. 3, which results from a separate analysis of the geometry of Mikado networks. In this analysis, random 2D networks of straight lines of length L_0 are generated with various densities, such to control l_c. The area of each cell is computed by image processing and $\bar{d} = \overline{\sqrt{A}}$ is evaluated. The figure supports the relation between the mean segment length and the mean cell diameter of eqn (1). With eqn (1) and the Kallmes–Corte relation, the point on the vertical axis in Fig. 2 corresponding to a given system results as $L_0/\bar{d} = 0.74\rho L_0$.

The minimum density below which a network does not form in the as-deposited state is given by the geometric percolation threshold for networks constructed by depositing randomly fibers of length L_0. The percolation threshold, ρ_l, is given by $\rho_l L_0 = 5.71$.[38,39] Hence, no network exists for $L_0/\bar{d} < 4.22$. This provides the lower bound for the range of the vertical axis in Fig. 2 in which points corresponding to as-deposited networks ($\bar{n} = 1$) may exist.

Fig. 2 shows that systems starting at $\bar{n} = 1$ evolve such that $L_0/\bar{d} \sim 1/\bar{n}$ (or $\bar{d} \sim \bar{n}$) at all stages of the evolution. This relation is a consequence of mass conservation. Consider the system at some stage of its evolution, in which the cell size is $\bar{d}$ and the degree of bundling is $\bar{n}$. The total number of chains in the model can be computed as $\rho L^2/L_0$, where ρL^2 is the total length of fiber in the model (or projected area $A = L^2$). On the other hand, the number of chains can be also estimated based on the perimeter $\wp$ of the bundled network, *i.e.* the total length of bundles in the model at given time, as $\bar{n}\wp/L_0$. Hence, $\rho L^2/\bar{n}\wp$. The total perimeter of the bundled network can be also evaluated as the perimeter of the representative cell times the number of such cells. Considering that the perimeter of the mean cell is proportional to $\bar{d}$, it results that: $\wp \sim L^2/\bar{d}$. Replacing this expression for $\wp$ in the previous relation involving $\bar{n}$, one obtains:

$$\bar{n} \sim \rho\bar{d}, \quad (2)$$

which provides conceptual support for the numerical results in Fig. 2.

It is observed in simulations that systems with larger initial ρL_0 lead to the formation of cellular structures, while systems with smaller ρL_0 disintegrate (Fig. 1). This is shown schematically in Fig. 2. The boundary separating the two types of behavior cannot be predicted based on theoretical considerations at this stage.

It is instructive to analyze the variation of the energies involved (axial, bending and adhesion) during the structural evolution of a network starting from the as-deposited state. The total axial energy is at all times much smaller than all other energies (below 5% of the total energy).

The adhesion energy is expected to be proportional to the total length of bundle in given state, $\wp$, times the adhesion energy per unit length of a bundle of size $\bar{n}$. This bundle-scale adhesion energy can be evaluated as the energy per contact between two fibers, γ, times the number of binary contacts in the bundle, $n_c(\bar{n})$. Harborth[40] has shown that the maximum number of contacts in a packing of n congruent circles is:

$$n_c(n) = 3n - \sqrt{12n - 3}. \quad (3)$$

Therefore, the adhesive energy stored within a perfect bundle of $\bar{n}$ filaments, per unit length of the bundle, is $\gamma\left(3\bar{n} - \sqrt{12\bar{n} - 3}\right)$. The negative term in the parenthesis has the physical meaning of a surface tension. Therefore the total adhesion energy reads:

$$E_a \sim \gamma n_c(\bar{n})\wp \sim \frac{\gamma n_c(\bar{n})}{\bar{n}}. \quad (4)$$

Fig. 4(a) shows the mean adhesion energy per fiber length σ, $E_{a\sigma}$, normalized by $\left(\frac{\gamma\sigma n_c(\bar{n})}{\bar{n}}\right)$ *vs.* $\bar{n}$ for all systems shown in Fig. 2. This numerical result is in agreement with eqn (4).

The variation of the bending energy during relaxation is shown in Fig. 4(b). The energy increases fast at the beginning of the process and then remains approximately constant throughout the deformation. The initial increase is due to the bending of initially straight fibers in the vicinity of the contact points, under the action of the adhesive forces. The subsequent behavior is more difficult to understand on theoretical grounds.

Fiber kinematics is of importance in order to understand the mechanisms of structural evolution. Three main fiber rearrangement modes are identified, as follows:

(i) Rigid rotation/translation of fibers. This fiber motion mode implies that filaments move as rigid bodies, as shown in Fig. 5(a). Driving is due to the small, but non-vanishing moments resulting from the adhesive interaction at contact points, M_i. Each of these moments tends to align the respective pair of fibers, closing the acute angle defined by them. Since fiber

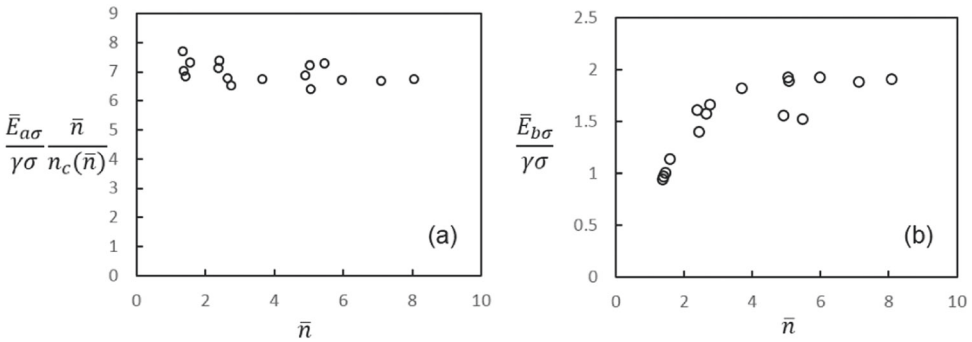

Fig. 4 Variation of the system average (a) adhesion and (b) bending energies with the bundle size during the evolution of the four systems shown in Fig. 2. The energies are reported per length of fiber equal to σ, and are normalized by the adhesion energy of two fibers in contact over length σ, *i.e.* $\gamma\sigma$. The adhesion energy is multiplied by the non-dimensional $\bar{n}$-dependent group of eqn (4).

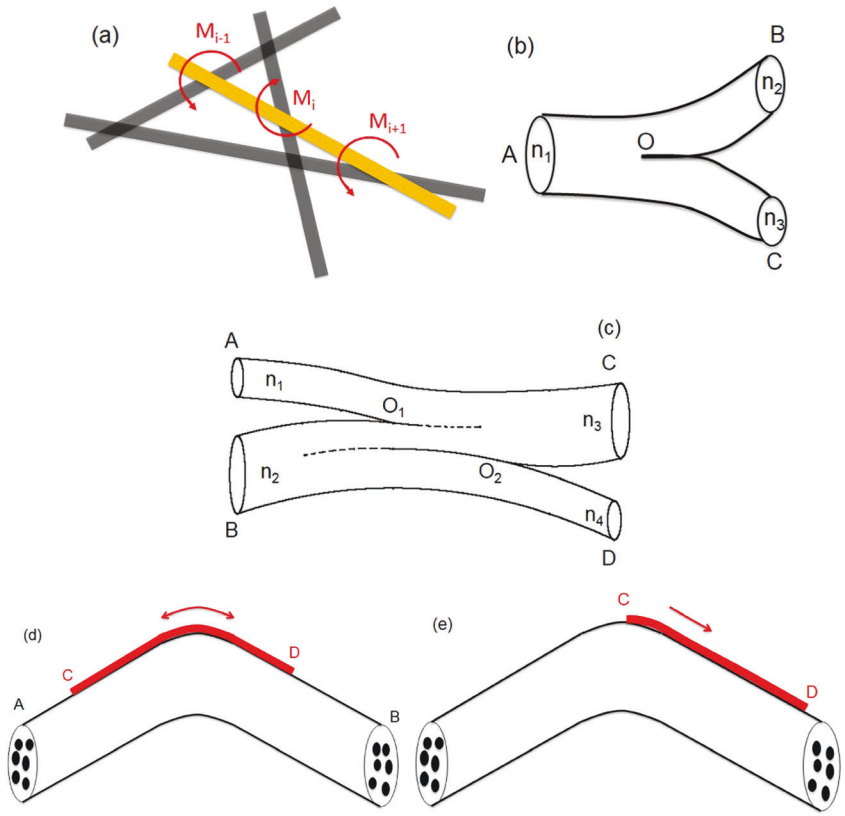

Fig. 5 Structural evolution modes for bundles and for individual fibers. (a) shows a rigid rotation mode, (b) and (c) show bundling and unbundling for two configurations, and (d) and (e) show reptation of individual fibers. The orange filament in (a) is loaded by moments that tend to close the acute angle at each fiber crossing. The bundle of size n_1 in (b) either peels off forming two bundles of smaller size, n_2 and n_3 ($n_1 = n_2 + n_3$), or re-bundles, such that node O, with connectivity $z = 3$, moves left or right. The configuration in (c) contains two nodes with $z = 3$ that may move past each other without interference. In (d) and (e) the red fiber slides relative to the rest of the bundle. The fiber can be on the outside of the bundle, as shown here, or inside. State (d) is stable since no driving force for fiber motion exists. In state (e) the fiber is driven to the right by the gradient of bending energy.

crossings are random, both the magnitude and direction of these moments is random. This motion mode becomes less efficient as the fiber length increases since the effective moment rotating the fiber is $\sum M_i$, which decreases as the number of the random, uncorrelated terms in the sum increases. Therefore, this mechanism is expected to apply only in the case of short and stiff fibers and in the limit of vanishing friction.

(ii) Bundling and unbundling. Two bundles of n_1 and n_2 fibers merge into a larger bundle of $n_1 + n_2$ fibers, which we call a 'handle' for the respective junction. The contact point may travel in both directions along the handle leading to bundling and unbundling (Fig. 5(b)). The handle O_1O_2 in Fig. 5(c) splits on the left side into two bundles of size n_1 and n_2, and on the right side into two bundles of size n_3 and n_4, with the obvious

conservation relation $n_1 + n_2 = n_3 + n_4$. This example demonstrates that nodes with $z = 3$ may travel past each other (by the motion of O_1 and O_2 in either direction). This structural evolution mode is not affected by friction and is the dominant evolution mechanism for the type of networks discussed in this article.

(iii) Reptation. Filaments are able to slide along the contour of bundles. This is shown schematically in Fig. 5(d) and (e). This mode is driven by the adhesive and bending energy difference (the chemical potential difference) between the two ends of the respective filament. Thermal fluctuations play no role in the reptation of athermal filaments. Fiber CD in Fig. 5(d) has ends C and D in regions of bundle AB of zero curvature. Hence, the bending energy at the two ends of CD is zero. If in addition, the adhesive energy of the two ends is equal, there is no driving force for reptation. The opposite situation is shown in Fig. 5(e), where fiber CD is driven to the right by the gradient of bending energy. An energy barrier prevents the reptation of fiber CD from the configuration in Fig. 5(e) to that in Fig. 5(d). Hence, fibers longer than the mean segment length of the network of bundles tend not to reptate, while short fibers reptate to the nearest state in which the energy difference between their ends vanishes.

4.2 Phase diagram of stable network states

We characterize the system of fibers with adhesion using two non-dimensional parameters: ρL_0 and

$$\Psi = \frac{\gamma L_0^2}{E_0 I_0}. \quad (5)$$

Ψ can be rewritten as $\Psi = L_0^2/L_{EC}^2$, where L_{EC} is the elasto-capillarity length introduced by Bico,[6] which captures the physics of bending-dominated elasticity in presence of surface forces.[41] Also, in ref. 27 the length scale $L_{EC} = \sqrt{E_0 I_0/\gamma}$ is identified as the key parameter controlling CNT structures stabilized by adhesion.

Networks with a broad range of parameter values are considered and evolved until energy stabilization. A summary of all simulation results is presented in Fig. 6. The figure shows a map of the resulting structures in different regimes of system parameters ρL_0 and Ψ. The map is bounded on the left by $\rho_l L_0 = 5.71$. For $\rho L_0 < \rho_l L_0$ no network forms upon fiber deposition and hence no further fiber organization is possible. Networks with $\rho L_0 > \rho_l L_0$ either remain locked in the initial, as-deposited state, or evolve. Crosses indicate simulated structures which remain in the as-deposited state, circles indicate simulations in which network disintegration occurs, while filled squares indicate cases in which a cellular network of bundles develops. The boundary between the cellular networks and disintegrating structures regions is defined based on simulation results. The boundary between evolving and locked structures is defined numerically and justified theoretically, as described below.

To identify the conditions under which the as-deposited network starts evolving under the action of adhesion, we consider

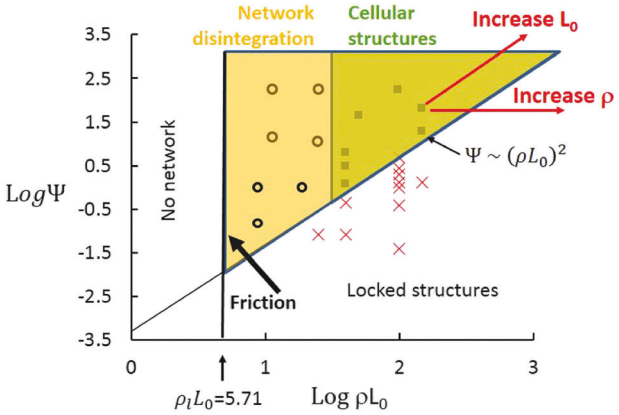

Fig. 6 Map indicating the expected structure of the network for various values of parameters ρL_0 and Ψ. No network forms for $\rho L_0 < \rho_l L_0$, while below the line of slope 2 defined by $\Psi \sim (\rho L_0)^2$, the as-deposited network does not evolve. The colored domains correspond to evolving networks which either disintegrate or form cellular structures. The symbols indicate states which have been simulated. Red crosses indicate non-evolving locked structures, open circles indicate networks that disintegrate and filled squares correspond to the formation of cellular structures. It is also indicated that increasing the filament length moves a point in this map further into the cellular domain, parallel to the boundary with the locked structures region, while increasing the density at constant fiber length transforms the structure into a locked state.

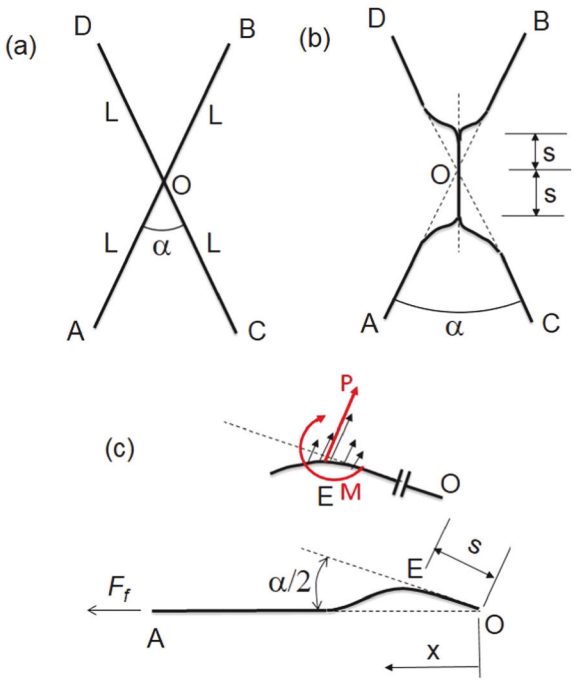

Fig. 7 Initial (a) and relaxed (b) configurations for two crossed fibers in contact at O. The two fibers bend and slide along their contour to accommodate adhesive contact along a segment of length 2*s* in the vicinity of O. (c) Shows a detail of one of the fibers in the vicinity of O, and the adhesive forces in the vicinity of *E*. Their resultant force *P* and moment *M* (shown in red) drive the change of shape of fiber OA.

two fibers of the network in contact at O and making an angle α (Fig. 7(a)). These fibers are in contact with other filaments at points not shown in the figure. Adhesion tends to bundle

these filaments, which is however restrained by their interactions with other fibers in the model. The boundary conditions in this case require that points A and B move during relaxation along line AB and likewise, C and D remain on the original line CD (Fig. 7(a)). Hence, filaments have to slide along their contour to accommodate the relative fiber rotation and bending in the vicinity of the contact point. This leads to the configuration of Fig. 7(b) in which the filaments stick over a length $2s$ in the vicinity of point O.

Fig. 7(c) shows the region of one of the fibers close to point O in Fig. 7(b). Segment OE rotates by $\alpha/2$ to adhere to filament OC. This is caused by the distribution of adhesive forces in the vicinity of point E, as shown schematically in the inset to Fig. 7(c). The mechanical equivalent of this distribution is the force P and moment M.

The bending energy stored in the filament can be evaluated as:

$$E_b = 2E_0I_0\frac{(\alpha/2)^2}{L-s} + 6E_0I_0\frac{s^2}{(L-s)^3}\sin^2\frac{\alpha}{2} + 3E_0I_0\frac{s}{(L-s)^2}\alpha\sin\frac{\alpha}{2}, \quad (6)$$

This expression results by solving the beam equation for the configuration in Fig. 7(c) under the boundary conditions: the deflection at E is $s\ \sin\frac{\alpha}{2}$, the rotation at E is $\alpha/2$, while at A, both deflection and rotation vanish. Segment AE stores bending energy.

The energy of adhesion corresponding to this filament is:

$$E_c = \frac{1}{2}\gamma s, \quad (7)$$

and the work performed against the far field friction (if any) is:

$$W_f \approx F_f s\ \sin^2\frac{\alpha}{4}. \quad (8)$$

Eqn (8) results by evaluating the change of the length of the beam from the straight to the current configuration shown in Fig. 7(c). Taking the derivative of $E_b - E_c + W_f$ with respect to s, the condition for the onset of relaxation result as:

$$\alpha^2\left(a + b\hat{F}_f\right) < \frac{\gamma L^2}{E_0I_0}, \quad (9)$$

where a and b are numerical coefficients of order unity, $\hat{F}_f = F_fL^2/E_0I_0$ and the approximation $\sin\alpha \approx \alpha$ was used. L represents the length of fiber between two successive contact points and is equal to the mean segment length, l_c. Using the Kallmes–Corte relation, $l_c = \pi/2\rho$, eqn (9) can be arranged as:

$$\Psi > (\rho L_0)^2 f(\hat{F}_f,\alpha). \quad (10)$$

Function f in eqn (10) is linear in the normalized friction force (eqn (9)). If the friction force is proportional to the number of contacts along the fiber (*i.e.* $\frac{L_0}{l_c} \sim \rho L_0$), $\hat{F}_f \sim 1/\rho$. In the absence of friction, $\hat{F}_f = 0$, and the condition for the initiation of system evolution becomes:

$$\Psi \sim (\rho L_0)^2. \quad (11)$$

The constant of proportionality in eqn (11) is linear in α^2. Extrapolating to the scale of the entire network analytically is not straightforward because fibers cross at angles forming a broad distribution. However, we conjecture that rearrangement should take place at a sufficient number of crossing points in order for the entire structure to re-organize. Hence, the factor containing α should be replaced at the scale of the entire network with a system average constant.

This analysis indicates that the boundary between locked and evolving structures should be described by eqn (11). This relation is shown in Fig. 6 by the diagonal line of slope 2. We observe that numerical results support this result. Further, eqn (9) and (10) indicate that accounting for inter-fiber friction would move the boundary between locked and evolving structures towards larger Ψ, therefore inhibiting system self-organization.

It is of interest to discuss the results in Fig. 6 in relation to specific filamentary systems. A given filament type is characterized by the elastocapilarity length L_{EC}. Networks of various densities and of various fiber lengths can be constructed with such filaments. Considering that $\Psi = {L_0}^2/{L_{EC}}^2$, any point of the map in Fig. 6 can be represented as $\log\Psi = 2\log\rho L_0 - 2\log\rho L_{EC}$. Based on this relation and the data (which correspond to vanishing friction between fibers), the boundary separating locked and evolving structures corresponds to $\rho L_{EC} = 44.6$. Therefore, for a specific type of fiber defined by L_{EC}, network densities $\rho > 44.6/L_{EC}$ correspond to locked structures, while $\rho < 44.6/L_{EC}$ correspond to evolving structures. The characteristic length L_{EC} can be evaluated based on literature data for various nanoscale filaments. For example, the adhesion energy per unit length of contact between two microtubules, γ, was reported to range from 2×10^{-14} to 17×10^{-14} J m^{-1} function of the ionic strength of the solution.[42] With $E_0I_0 = 9 \times 10^{-24}$ Nm^2 reported for individual microtubules[43] of 25 nm outer diameter one obtains L_{EC} in the range 7 to 20 μm. Single wall carbon nanotubes (10,10) of diameter 1.4 nm have $E_0I_0 \approx 3.2 \times 10^{-25}$ Nm^2 [44] and $\gamma \approx 2.9 \times 10^{-9}$ J m^{-1} [45] which leads to $L_{EC} \approx 10$ nm. Likewise, polyacrylonitrile (PAN) fibers of ~300 nm diameter produced by electrospinning exhibit $\gamma \approx 1 \times 10^{-9}$ J m^{-1},[46] which, with a measured $E_0 = 3$ GPa,[47] leads to $L_{EC} \approx 34$ μm. Note the much smaller value of L_{EC} obtained for carbon nanotubes which indicates, in agreement with experimental observations, that network self-organization should be prevalent in these systems.

4.3 Network design considerations

The data presented in Section 4.2 can be used to guide the design of fiber networks with adhesion. In particular, it is of practical interest to understand the effect of parameters controllable in experiments, such as ρ and L_0, on the final state of the relaxed structure. The map indicates that increasing the filament length L_0 moves a given point of the map towards the regime of cellular structures (shown in Fig. 6 by a red arrow). Hence, working with networks of longer fibers increases the probability to obtain a cellular network of bundles upon full system relaxation. Volkov and Zigilei[28] also report this effect and observe that increasing the fiber length stabilizes the resulting structure of bundles.

On the other hand, increasing the density promotes locking. Points in the map corresponding to systems with increasing ρ,

but constant Ψ, move horizontally (shown in Fig. 6 by a red arrow). Clearly, decreasing γ or increasing the bending rigidity of fibers brings the system into the range of locked structures.

In practical situations, the as-deposited filaments could be fiber bundles. The map in Fig. 6 can be used for these cases too, since the relevant mechanics remains unchanged. However, the values of ρL_0 and Ψ to be used in this context become dependent on the size of the as-deposited bundles, n. Parameter ρL_0 is to be replaced by $\rho_b L_0$, where ρ_b is the density of as-deposited bundles, while γ should be replaced by $\gamma_b(n)$ which represents the variation of the adhesion energy when two bundles, each of size n, merge into a single bundle of size $2n$. Eqn (3) can be used to evaluate $\gamma_b(n)$:

$$\gamma_b(n) = \left(2\sqrt{12n-3} - \sqrt{24n-3}\right)\gamma \qquad (12)$$

With eqn (12), parameter Ψ_b (which replaces Ψ in this evaluation) becomes:

$$\Psi_b = \frac{\gamma_b(n)L_0^2}{E_0 I} = \frac{\gamma_b(n)}{\gamma n}\Psi \approx \frac{2}{\sqrt{n}}\Psi, \qquad (13)$$

where the moment of inertia of the bundle, I, was evaluated as $I = nI_0$, since the fibers in the bundle are free to slide axially during bundle bending.

Since $\Psi_b \ll \Psi$, the adhesive interaction of two bundles is much weaker than the interaction of two fibers. Therefore, as-deposited networks which are composed from bundles are unlikely to evolve into cellular networks of fiber bundles.

5. Cellular networks are stabilized by triangular structures of fiber bundles

Simulations indicate that in the last stages of evolution of a network of bundles, triangular features form at a majority of the network nodes. Fig. 8 shows a small region of a much larger cellular network which exhibits such triangles at each node. Each edge of the triangle is made from multiple fibers. The bundles outside the triangular regions, *i.e.* the cell walls, tend to become straight. Therefore, the triangles concentrate the entire bending energy of the cellular network.

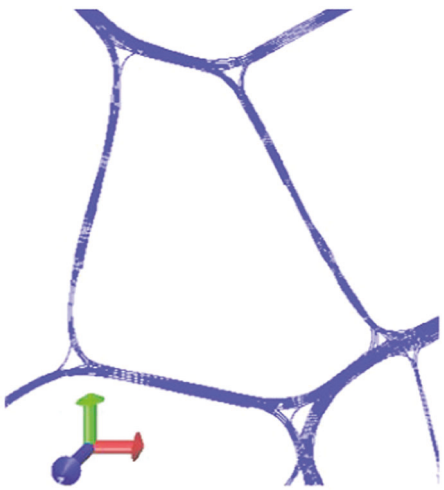

Fig. 8 Section of a cellular network showing triangular features developing at all network nodes.

In this section we outline the mechanism by which these triangular features stabilize cellular structures. Give their importance, we also discuss the relation between the size of the bundles merging into a node and the structure and energy of the triangle that stabilizes the respective node.

The physical picture emerging from this analysis is that adhesion drives the ensemble of fibers towards disintegration in all cases. Cellular networks of fiber bundles are stabilized when the kinetics of formation of nodal triangular features is faster than the kinetics of disintegration.

5.1 Cellular network stability analysis

We consider first cases in which the fiber length, L_0, is much larger than the cell size, d. The overall structural evolution of the cellular network requires that network nodes move and hence mandates that triangles slide along network bundles. Consider that a driving force exists for triangle ABC in Fig. 9(a) to move along bundle A′C′ to the right. In this process, bundles AB and AC merge at A (segment AA′ becomes longer), while

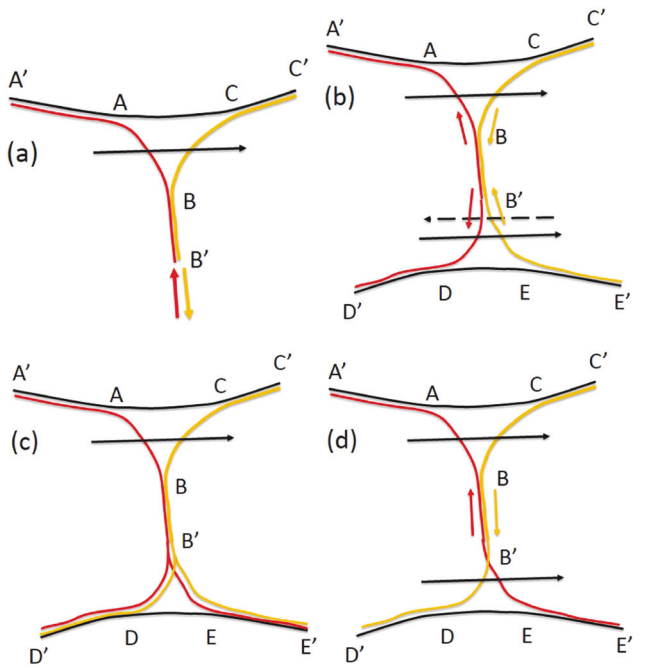

Fig. 9 Schematic representation of the correlated motions of two neighboring triangular structures. (a) The motion of triangle ABC along bundle A′C′ (in the direction shown by the black arrow) requires bundling at A, unbundling at C, and relative sliding of the red and orange sub-bundles along BB′. Panels (b) and (c) show the three possible correlated motion modes of two neighboring triangles (ABC and B′DE): (b) improbable case in which all fibers separating from AA′ (red) continue into DD′. This configuration is locked; (c) most probable configuration in which fibers separating from AA′ and CC′ form part of both DD′ and EE′. This configuration is locked. (d) Improbable case in which all fibers separating from AA′ (red) form part of EE′ and all fiber separating from CC′ (orange) form DD′.

bundles BC and AC separate at C (segment CC′ becomes shorted). This requires minimal energy expenditure since no relative sliding is involved and only the adhesive energy associated with bundling (at A) and unbundling (at C) varies. Actually, this energy difference drives the motion of the node. However, the process requires relative sliding of sub-bundles within bundle BB′ (indicated by colored arrows). Sliding in BB′ takes place against inter-fiber friction and has to be accommodated by a reciprocal evolution of the triangle located at the other end of segment BB′. Hence, in order to evaluate the ability of triangle ABC to move, it is necessary to consider the correlated evolution of multiple neighboring nodes of the cellular network. Fig. 9(b)–(d) show schematically three possible such configurations. In all these cases, we consider the fiber length L_0 to be larger than the cell size d and much larger than the length of any segment in Fig. 9. Fig. 9(b) shows the extremely improbable case in which all fibers separating from AA′ at A (red segment AB) continue into B′D and DD′, and all fibers forming CB also form B′E and EE′. Consider that triangle ABC moves to the right as shown by the black arrow. Under these circumstances, moving triangle B′DE to the right, as shown by the black continuous arrow, is impossible since filament length has to be provided at both A and D and has to be eliminated from both C and E, which violates mass conservation. The 4 small arrows parallel to the respective bundles indicate the direction of sliding mandated by the imposed motion of triangles ABC and B′DE. This topological incompatibility is eliminated if triangle B′DE moves to the left, as indicated by the dashed black arrow. However, in this case segment BB′ is subjected to bending and its length has to increase which, again, violates mass conservation. The most probable configuration is shown in Fig. 9(c) where fibers forming AB as well as the fibers forming BC continue into both bundles B′D′ and B′E′, as indicated schematically by the colors used. This case is locked for reasons identical to those outlined in relation to the case in Fig. 9(b). The only configuration in which both nodes B and B′ can move without violating mass conservation and without bending or elongating BB′ is shown in Fig. 9(d). The two triangles ABC and B′DE have to move in the same direction and their motion is accommodated by the relative sliding of the sub-bundles of BB′ shown in red and orange, as indicated by the two small colored arrows (Fig. 9(d)). If A′C′ and D′E′ are parallel, the length of BB′ does not increase. This is the only energetically neutral and topologically allowable correlated motion mode of two neighboring triangles. However, the probability of existence of such configuration is extremely small (and decreases fast with increasing the size of the respective bundles) since it is necessary that all fibers in AB form also B′E and all fibers in BC also form B′D. This analysis demonstrates that structural evolution of a cellular network of bundles which has triangles at all nodes is topologically impossible. Therefore, the nodal triangles are the key geometric features that stabilize the cellular network.

If the fiber length L_0 is smaller than the cell wall length, BB′, conditions exist for network disintegration. Under the action of adhesion, segments AD and CE collapse into an isolated bundle of length L_0, and a similar process takes place at all cell walls leading to network disintegration.

This discussion indicates that if triangles form at all nodes of the network before the cells grow to a size d comparable with L_0, the cellular network of bundles becomes stable. Otherwise, the network decomposes into isolated bundles. Since adhesion always drives the network towards disintegration, the formation of stable cellular networks requires that the kinetics of formation of nodal triangular features is faster than that of cell growth and network disintegration.

Further insight into the structural evolution of the network and formation of nodal triangles can be obtained from an entirely geometric analysis of cell evolution, as discussed in the Appendix. A 'stability index' is defined indicating under what conditions a cell is stable. A cell with triangles at all nodes is always stable, independent of the number of cell walls or cell size. The cellular network is globally stable when all of its cells are stable. This method allows identifying how close to global stability is a cellular structure in some intermediate state of its evolution.

It is interesting to draw a parallel between these triangles formed by fiber bundles, with role in the stabilization of cellular filamentary structures, and the Plateau triangles observed in foams.[48] In a liquid foam, all intersections of cell faces are decorated with regions of fluid with triangular cross-section known as Plateau triangles. Liquid rich domains are found at triple points where multiple 3D cells meet. These Plateau triangles are necessary for the stability of the foam and store the largest amount of fluid in the structure. While surface tension plays the stabilizing role in the Plateau triangles case, in the problem discussed here the stabilization effect is due to the constrained kinematics of filaments.

5.2 Structure and energetics of triangles of fiber bundles

Given the central role of triangular structures in the stability of cellular networks, and for completeness, it is necessary to fully characterize them from structural and energetic points of view.

The structure of a triangle depends on the size of the 3 external bundles and the angles between them. Consider the structure in Fig. 10, with external bundles of size n_1, n_2 and n_3 forming angles α_1, α_2 and α_3. The sub-bundles connecting

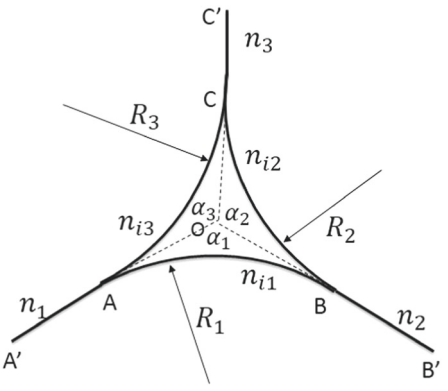

Fig. 10 Parameters defining a triangle of fiber bundles.

nodes A, B and C are of size n_{i1}, n_{i2} and n_{i3} and the obvious conservation conditions of eqn (14) hold.

$$n_1 = n_{i1} + n_{i3},$$
$$n_2 = n_{i1} + n_{i2},$$
$$n_3 = n_{i2} + n_{i3} \quad (14)$$

Several observations can be made by inspection. Bundles AB, BC and AC forming the triangle are loaded in pure bending and hence are arcs of circle of radii R_1, R_2 and R_3. Since these circles must be tangent to each other at A, B and C, segments OA, OB and OC are also of equal length, l_{tr}. If the incoming bundles AA′, BB′ and CC′ are straight, *i.e.* the entire bending energy is concentrated in the triangle, the bending moments loading the three edges of the triangle are equal, M_{tr}.

The equilibrium configuration results by minimizing the total energy, for given bundle sizes and set of angles, relative to the size of the triangle, l_{tr}. The bending moment results:

$$M_{tr} = \sqrt{\frac{2\gamma E_0 I_0}{\pi}B} \quad (15)$$

and the total bending and adhesive energies of the structure are:

$$E_{b\,tr} = \frac{\pi}{2}M_{tr} = \sqrt{\frac{\pi\gamma E_0 I_0}{2}B} \quad (16)$$

$$E_{atr} = CL_{tr} - E_{btr}, \quad (17)$$

where

$$C = \sum_{k=1,3} \gamma n_c(n_k)$$

$$B = \sum_{k=1,3} n_{ik} n_c(n_k) \tan\frac{\pi - \alpha_k}{2} - n_{ik} n_c(n_{ik})(\pi - \alpha_k) \quad (18)$$

and L_{tr} is the length of segments OA′, OB′ and OC′ and scales proportional with the mean segment length of the cellular network.

6 Conclusions

The structural evolution of networks of non-crosslinked filaments self-organized by adhesion is discussed in this article. The driving force for system evolution is provided by the interplay between bending and adhesion energies. Since fibers are free to relax axially, the axial deformation energy is negligible. At small fiber densities and/or small filament lengths, ρL_0, the formation of bundles leads to the loss of connectivity of the network which eventually disintegrates into isolated fiber bundles. Cellular networks of bundles form at large ρL_0 and large values of the adhesion parameter Ψ. Such cellular networks are qualitatively different from non-crosslinked and cross-linked networks without adhesion. These are stabilized by the formation of a characteristic triangular structure of fiber bundles at all nodes. The stabilization mechanism and the configuration of these triangles are discussed in detail. If Ψ is sufficiently small compared to $(\rho L_0)^2$, adhesion is too weak to drive network self-organization, and the structure remains in the unbundled state. This analysis provides a comprehensive physical picture of structural evolution and bundling under the action of adhesion in filamentary structures, with applications to a diverse set of systems of current interest.

Conflicts of interest

There are no conflicts to declare.

Appendix

In this appendix we present a geometric method to predict the stability of a generic cell of the cellular network at some intermediate state of its evolution. A 'stability index' is introduced

Table 1 Structural evolution of cells with no nodes stabilized by triangles in the initial state. The initial structures are shown in column 2, with the number of edges of the cell, N_e, indicated in column 1. The initial structures evolve by holding the nodes fixed and allowing the total contour length to increase. Column 3 shows the transformed structure, while columns 4, 5 and 6 indicate the values of parameters N_{i1}, N_{i2}, the number of triangles resulting upon structural evolution, and the corresponding cell stability index, CSI (eqn (A1))

N_e	Initial cell shape	Relaxed cell shape	N_{i1}; N_{i2}	No. triangles	CSI
3	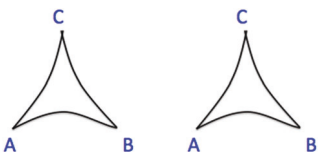		0; 0	1	3
4	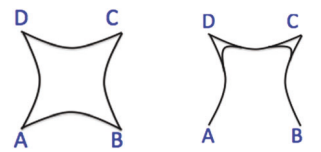		0; 0	2	4
4	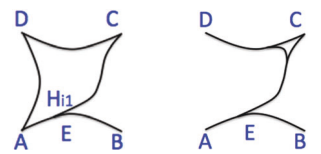		1; 0	1	3
4	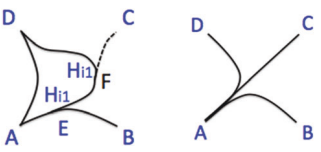		2; 0	0 (collapse)	2
5	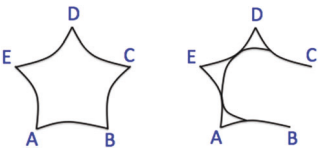		0; 0	3	5
5	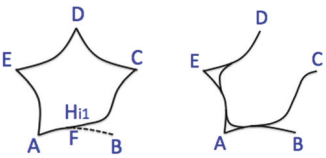		1; 0	2	4

which can be used to determine whether a cell is stable in the current configuration or not.

A cell is defined by the number of edges, N_e, and the nature of the nodes. Table 1 shows a classification of cells in these terms. The discussion uses terminology introduced in Section 4.1 referring to Fig. 5(b). Specifically, a bundle that splits into two sub-bundles (bundle AO in Fig. 5(b)) is called a 'handle'. Bundles (or handles) forming the walls of a cell are called 'internal,' while all others are called 'external.'

A number of observations can be made based exclusively on the geometry. Triangular cells (N_e = 3) may take only one configuration and only the external bundles can be handles. The triangle is stable only in the concave configuration shown in Table 1, line 1.

Multiple configurations are possible for N_e = 4 (lines 2 to 4 in Table 1). We evaluate their stability by the following procedure: the end nodes, A, B, C and D, are held fixed and the density of the cell is allowed to increase by sliding in, along its contour, one of the bundles going through the end nodes. The resulting structures for the four configurations shown for N_e = 4 are represented in the third column of Table 1, lines 2 to 4. Only one of the multiple (but equivalent) resulting configurations corresponding to each initial state is shown. Two possibilities exist: either the cell collapses, or it develops into a simpler structure that contains triangles. The number of resulting triangles depends on the number of the initial cell edges that are handles. A cell edge bundle that splits at one end is called ''internal handles of order 1'' and is denoted by H_{i1}. N_{i1} represents the number of such handles in the given cell. The structure on line 2 of Table 1 has only external handles, that on line 3 has one internal handle of order 1 (segment AE), while that on line 4 has 2 internal handles of order 1 (segments AE and EF).

This argument applies to cells with any number of edges; a further example is shown in Table 1, lines 5 and 6, for N_e = 5. The situation is similar: the structure with no internal handles (line 5 of Table 1) evolves into a simpler structure with 3 triangles, while as the number of internal handles increases, the number of triangles in the final structure decreases. A collapsed structure (the cell disappears) results for N_e = 5 and N_{i1} = 3.

Further, we consider situations in which some of the nodes of the original cell are stabilized by triangles. A family of related configurations based on the N_e = 4, N_{i1} = 1 of Table 1 (line 3) is shown in Table 2. A case with one stabilized node is shown on the first line of Table 2. This example has N_e = 5 after the introduction of the triangle at node C and of edge FG. The number of internal handles in this case is N_{i1} = 3. This structure may evolve into the configuration shown in column 3, line 1, of Table 2, having a single triangle. To envision this transformation, hold the outer handle nodes A, B, C and D fixed and allow segment AD to move into the cell and adhere to AEFGD. As the number of stabilized nodes increases, both N_e and N_{i1} increase and this stabilizes the initial state. ''Internal handles of order 2'' (denoted H_{i2}) are bundles that split into sub-bundles at both ends and appear as edges connecting two triangles. Their number in the cell is indicated by N_{i2}. An example is segment GH in the initial structure on line 2, column 2 of Table 2. This structure has N_e = 6, N_{i1} = 3 and N_{i2} = 1 and is stable. It has two triangles and one external handle. Even if the external handle node is allowed to move into the cell, node E may be eliminated, but the general structure of the cell does not change.

Table 2 Structural evolution of cells with nodes stabilized by triangles in the initial state. Parameter specification identical to that in Table 1

N_e	Initial cell shape	Relaxed cell shape	N_{i1}; N_{i2}	No. triangles	CSI
5	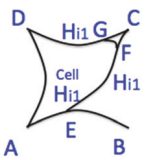	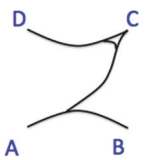	3; 0	0 (collapse)	2
6	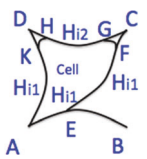	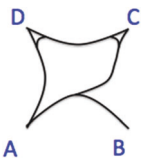	3; 1	Stable cell of type 1	1
7	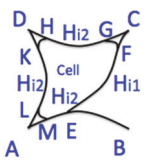	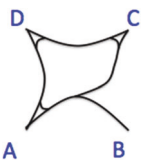	1; 3	Stable cell of type 0	0
8	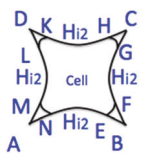	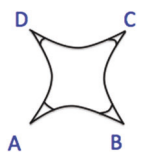	0; 4	Stable cell of type 0	0

A cell with one external handle and all other nodes being stable is denoted as ''Stable cell or type 1''. Eliminating the external handle and placing triangles at all nodes of the original structure fully stabilizes the cell. The stable structure on line 4 of Table 2 has $N_e = 8$, $N_{i1} = 0$ and $N_{i2} = 4$. We denote this structure as ''Stable cell of type 0.''

This geometric analysis indicates two important features of cellular structures:

– The triangle is the most stable structure and is needed in order to stabilize cells with number of edges larger than 3,

– It is possible to devise an index, the ''cellular stability index,'' CSI, which indicates the type of structure resulting from any initial cell. This index is defined as:

$$\mathrm{CSI} = N_e - N_{i1} - 2N_{i2}, \qquad \text{(A1)}$$

and its values for the cells in Tables 1 and 2 are shown in the respective tables.

CSI indicates the number of triangles in the relaxed structure and whether the cell is stable in the current configuration or not:

(1) If CSI $\geq$ 2, the cell is not stable in the current state. If CSI = 2, the cell collapses. If CSI $>$ 2, CSI $-$ 2 represents the number of triangles of the structure that results upon cell evolution.

(2) Cells with CSI = 1 and CSI = 0 correspond to stable cells of types 1 and 0, respectively (Table 2).

Acknowledgements

This work was supported by the NSF through grant CMMI-1634328 and by NASA through grant NNX16AE03G. We thank Mr Vineet Negi for useful discussions and the Center for Computational Innovation (CCI) of Rensselaer Polytechnic Institute for providing access to computational resources.

References

1 D. J. S. Hulmes, *Collagen: Structure and Mechanics*, 2008, pp. 15–47.
2 V. R. Sherman, W. Yang and M. A. Meyers, *J. Mech. Behav. Biomed. Mater.*, 2015, **52**, 22–50.
3 J. Bico, *Nature*, 2004, **432**, 690.
4 M. De Volder and A. J. Hart, *Angew. Chem., Int. Ed.*, 2013, **52**, 2412–2425.
5 R. W. Style, A. Jagota, C. Y. Hui and E. R. Dufresne, *Annu. Rev. Condens. Matter Phys.*, 2017, **8**, 99–118.
6 A. V. Linares, F. Vandevelde, J. Pantigny, A. Falcimaigne-Cordin and K. Haupt, *Adv. Funct. Mater.*, 2009, **19**, 1299–1303.
7 S. Cranford, H. Yao, C. Ortiz and M. J. Buehler, *J. Mech. Phys. Solids*, 2010, **58**, 409–427.
8 A. Thess, R. Lee, P. Nikolaev, H. Dai, P. Petit, J. Robert, C. Xu, Y. H. Lee, S. G. Kim and A. G. Rinzler, *Science*, 1996, **273**, 483–487.
9 A. Wierenga, A. P. Philipse, H. N. Lekkerkerker and D. V. Boger, *Langmuir*, 1998, **14**, 55.
10 M. Tempel, G. Isenberg and E. Sackmann, *Phys. Rev. E: Stat. Phys., Plasmas, Fluids, Relat. Interdiscip. Top.*, 1996, **54**, 1802.
11 S. Yunoki, H. Hatayama, M. Ebisawa, E. Kondo and K. Yasuda, *J. Biomed. Mater. Res., Part A*, 2015, **103**, 3054–3065.
12 A. G. Zilman and S. A. Safran, *Europhys. Lett.*, 2003, **63**, 139–145.
13 S. Bounoua, E. Lemaire, J. Ferec, G. Ausias and P. Kuzhir, *J. Rheol.*, 2016, **60**, 1279–1300.
14 M. Chaouche and D. L. Koch, *J. Rheol.*, 2001, **45**, 369–382.
15 L. Berhan, Y. B. Yi, A. M. Sastry, E. Munoz, M. Selvidge and R. Baughman, *J. Appl. Phys.*, 2004, **95**, 4335–4345.
16 J. N. Coleman, W. J. Blau, A. B. Dalton, E. Munoz, S. Collins, B. G. Kim, J. Razal, M. Selvidge, G. Vieiro and R. H. Baughman, *Appl. Phys. Lett.*, 2003, **82**, 1682–1684.
17 J. Liu, A. G. Rinzler, H. Dai, J. H. Hafner, R. K. Bradley, P. J. Boul, A. Lu, T. Iverson, K. Shelimov and C. B. Huffman, *Science*, 1998, **280**, 1253–1256.
18 J. P. Lu, *Phys. Rev. Lett.*, 1997, **79**, 1297.
19 R. C. Picu, *Soft Matter*, 2011, **7**, 6768–6785.
20 C. P. Broedersz and F. C. MacKintosh, *Rev. Mod. Phys.*, 2014, **86**, 995.
21 D. Poquillon, B. Viguier and E. Andrieu, *J. Mater. Sci.*, 2005, **40**, 5963–5970.
22 D. Rodney, M. Fivel and R. Dendievel, *Phys. Rev. Lett.*, 2005, **95**, 108004.
23 G. Subramanian and R. C. Picu, *Phys. Rev. E: Stat., Nonlinear, Soft Matter Phys.*, 2011, **83**, 056120.
24 S. Toll, *Polym. Eng. Sci.*, 1998, **38**, 1337–1350.
25 C. Van Wyk, *J. Text. Inst., Trans.*, 1946, **37**, T285–T292.
26 Y. Li and M. Kröger, *Appl. Phys. Lett.*, 2012, **100**, 021907.
27 Y. Li and M. Kröger, *Carbon*, 2012, **50**, 1793–1806.
28 A. N. Volkov and L. V. Zhigilei, *ACS Nano*, 2010, **4**, 6187–6195.
29 M. Xu, D. N. Futaba, T. Yamada, M. Yumura and K. Hata, *Science*, 2010, **330**, 1364–1368.
30 Y. Li and M. Kröger, *Soft Matter*, 2012, **8**, 7822–7830.
31 A. S. Shahsavari and R. C. Picu, *Phys. Rev. E: Stat., Nonlinear, Soft Matter Phys.*, 2012, **86**, 011923.
32 B. V. Derjaguin, V. M. Muller and Y. P. Toporov, *Prog. Surf. Sci.*, 1994, **45**, 131–143.
33 K. L. Johnson, *Contact mechanics*, Cambridge University Press, Cambridge, 1985.
34 B. N. Persson, *Surf. Sci. Rep.*, 2006, **61**, 201–227.
35 F. J. Schmied, C. Teichert, L. Kappel, U. Hirn and R. Schennach, *Rev. Sci. Instrum.*, 2012, **83**, 073902.
36 S. Plimpton, *J. Comput. Phys.*, 1995, **117**, 1–19.
37 O. Kallmes and H. Corte, *Tappi J.*, 1960, **43**, 737–752.
38 D. Stauffer and A. Aharony, *Introduction to percolation theory*, CRC Press, 1994.
39 J. Wilhelm and E. Frey, *Phys. Rev. Lett.*, 2003, **91**, 108103.
40 H. Harborth, *Elem. Math.*, 1974, **29**, 14–15.
41 J. N. Israelachvili, *Intermolecular and surface forces*, Academic Press, New York, 1991.

42 F. Hilitski, A. R. Ward, L. Cajamarca, M. F. Hagan, G. M. Grason and Z. Dogic, *Phys. Rev. Lett.*, 2015, **114**, 138102.
43 T. Hawkins, M. Mirigian, M. Selcuk Yasar and J. Ross, *J. Biomech.*, 2010, **43**, 23.
44 X. Guo and T. Zhang, *J. Mech. Phys. Solids*, 2010, **58**, 428–443.
45 T. Li, A. Ayari and L. Bellon, *J. Appl. Phys.*, 2015, **117**, 164309.
46 Y. C. Liu and D. A. Lu, *Plasma Chem. Plasma Process.*, 2006, **26**, 119–126.
47 M. Naraghi, P. V. Kolluru and I. Chasiotis, *J. Mech. Phys. Solids*, 2014, **62**, 257.
48 D. Weaire and S. Hutzler, *The Physics of Foams*, Oxford University Press, New York, 1999.

